Research on Chemical Intermediates (2020) 46:4173–4192
https://doi.org/10.1007/s11164-020-04199-4

Preferential oxidation of carbon monoxide in a hydrogen-rich gas stream over supported gold catalysts: the effect of a mixed ceria–zirconia support composition

Sasiporn Chayaporn[1] · Chachchaya Thunyaratchatanon[1,2] · Apanee Luengnaruemitchai[1,2,3]

Received: 27 December 2019 / Accepted: 16 June 2020 / Published online: 26 June 2020

Abstract

The effect of the ceria–zirconia (CeO_2–ZrO_2) support composition of a gold (Au) catalyst (Au/$Ce_{1-x}Zr_xO_2$, where x is the molar ratio), prepared by deposition–precipitation, on its catalytic activity was investigated in the preferential carbon monoxide (CO) oxidation. A maximum CO conversion level of 94% was obtained with 1% by weight Au/$Ce_{0.75}Zr_{0.25}O_2$ at 50 °C, while the presence of water and carbon dioxide in the feed stream had only a slight effect on the catalytic activity. Catalyst characterizations were performed to investigate the effect of the Ce:Zr molar ratios on the redox properties and physicochemical properties of the obtained Au/CeO_2–ZrO_2 catalysts. It was found that a certain amount of Ce in the Au/CeO_2–ZrO_2 catalyst promoted solid solution formation and facilitated the activity of Au^{3+} and Au^0 nanoparticles with a small crystallite size. The enhanced catalytic activity of Au/$Ce_{0.75}Zr_{0.25}O_2$ was attributed to the presence of more oxygen vacancies, easier reducibility, and appropriate amount of Au^{3+} species, as confirmed by Fourier transform Raman spectroscopy and hydrogen-temperature-programme reduction analyses, respectively. The catalytic activity showed a high stability for a long period of time (28 h).

Keywords PROX · CO conversion · Au catalyst · CeO_2–ZrO_2 · Solid solution

✉ Apanee Luengnaruemitchai
apanee.l@chula.ac.th

[1] The Petroleum and Petrochemical College, Chulalongkorn University, Bangkok 10330, Thailand

[2] Center of Excellence on Petrochemical and Materials Technology, Chulalongkorn University, Research Building, Phayathai Rd., Bangkok 10330, Thailand

[3] Center of Excellence on Catalysis for Bioenergy and Renewable Chemicals (CBRC), Chulalongkorn University, Phayathai Rd., Pathumwan, Bangkok 10330, Thailand

Introduction

Gold (Au) is normally considered as the most inert of all metals. However, since the pioneering work of Haruta [1], Au deposited on various metal oxides has been shown to have a high activity towards carbon monoxide (CO) oxidation. These Au-based catalysts have been shown to be very active and have received much attention for numerous applications, especially for proton exchange membrane fuel cell (PEMFC) applications using hydrogen (H_2) as an energy source. Typically, a fuel processor consists of a reformer, a water–gas shift (WGS) reactor, and a CO removal unit. An efficient method to reduce the CO content in the reformed gas is the preferential CO oxidation (CO-PROX). The attractive research area of Au catalysts in a variety of reactions, including the WGS [2], CO-PROX [3], and the oxidative steam reforming of methanol (OSRM) [4] reactions have been reported, but a careful preparation procedure is crucial in order to obtain the Au as well-dispersed nanoparticles (NPs) on the oxide support. The activity of a catalyst literally depends on the size and shape of the AuNPs, a strong contact between the AuNPs and the support, and a suitable selection of the support.

Ceria (CeO_2) has been regarded as one of the most ubiquitous supports in catalytic systems and has been widely used for many applications due to its remarkable redox properties and a high oxygen storage capacity (OSC). Recent studies [3, 5, 6] have shown that Au supported on reducible oxide supports, such as CeO_2, iron oxide (Fe_2O_3), and titania (TiO_2), exhibited a markedly enhanced CO-PROX performance. Among those supports, Au supported on nanocrystalline CeO_2 exhibited a catalytic activity of two orders of magnitude more than the Au/TiO_2 and Au/Fe_2O_3 catalysts [7], owing to the surface/interface structures. However, it has been well-documented that the Au particle size, composition, electronic structure, and facet structure of the noble metal and reducible oxide are considered as important factors in determining their catalytic performance [5, 8, 9].

Clearly, peripheral Au species are required for this reaction and the reaction rate will increase as the particle size is decreased. The main contention is the oxidation state of the Au as the active species. Although this includes Au^0 and $Au^{\delta+}$, the relation of the Au oxidation state to the CO oxidation activity remains unresolved. It has previously been reported that a high $Au^{\delta+}/Au^0$ ratio may be one of the important factors determining the catalytic activity of AuNPs [3]. A CeO_2 containing Au-based catalyst is able to oxidize CO molecules at a low temperature due to its high OSC and good redox properties. The CeO_2 NPs can stabilize cationic $Au^{\delta+}$ species and improve the charge transfer by redox processes, including the oxidation of Au^0 to $Au^{\delta+}$.

Modification of the CeO_2 support by addition of zirconium (Zr) has been intensively investigated in recent years as a means to obtain an improved thermal stability and a CeO_2–ZrO_2 solid solution formation [4, 10]. This can lead to the formation of mixed oxides with smaller crystallites, good redox properties [11], and an enhanced reducibility of Ce^{4+} compared to a single metal oxide [12]. However, the activity of Au catalysts on these mixed-metal oxide supports was found to be strongly dependent on not only the morphological structure of the mixed oxide but also on having

a suitable Ce:Zr atomic ratio in the mixed oxide and the preparation route used to obtain the solid solution [11, 12]. In recent years, mixed Ce–Zr oxides have been used as a support for Au catalysts in many reactions. We have recently investigated the catalytic activity performance in the OSRM [13] and SRM [14] reactions of Au and Au–Cu supported on mixed Ce–Zr oxides with Ce:Zr atomic ratios of 3:1 ($Ce_{0.75}Zr_{0.25}$), 1:1 ($Ce_{0.5}Zr_{0.5}$), and 1:3 ($Ce_{0.25}Zr_{0.75}$) prepared by co-precipitation (CP). The presence of an active uniform $Ce_{0.75}Zr_{0.25}$ solid solution was found to be clearly beneficial in terms of a high stability of the Au/$Ce_{0.75}Zr_{0.25}$ catalyst in the OSRM reaction at 350 °C [4]. Inspired by our previous work, the objective of the present study was to investigate the effect of Zr on the physicochemical properties and catalytic activity of Au/CeO_2–ZrO_2 for the CO-PROX.

Accordingly, a series of CeO_2–ZrO_2 supports of different atomic ratios of Ce:Zr were prepared by CP in order to obtain a defective fluorite structure and increased oxygen mobility. The supported Au catalysts were prepared by deposition–precipitation (DP) and their catalytic performance in the CO-PROX reaction in a H_2-rich stream was determined. The effects of the support composition and the feed stream composition on the catalytic performance of the supported AuNP catalysts were investigated, while the catalyst stability (deactivation) was evaluated. The relationship between the composition and structural properties of the catalyst and its catalytic performance was ascertained by diverse characterization techniques.

Experimental

Catalyst preparation

Procedures for synthesizing the Au-based catalysts followed previously published methods [11]. A series of CeO_2–ZrO_2 supports were prepared by CP using cerium (III) nitrate hexahydrate ($Ce(NO_3)_3{\cdot}6H_2O$; 99%, Sigma-Aldrich, CAS 10294-41-4) and zirconium (IV) oxychloride octahydrate ($ZrOCl_2{\cdot}8H_2O$; 98%, Sigma-Aldrich, CAS 13520-92-8). The atomic ratio of the two metals (Ce/Zr) was varied to obtain $Ce_{1-x}Zr_xO_2$ solid solutions, where x was 0, 0.25, 0.5, 0.75, or 1.0 atom ratio. The solution was then adjusted to pH 8–9 by adding an aqueous solution of 0.1 M Na_2CO_3 (99.5%, Sigma-Aldrich, CAS 497-19-8) and stirred for 1 h at 80 °C. The precipitate was dried at 110 °C for 12 h and calcined in air at 400 °C for 4 h.

The DP technique was used to load 1% by weight (wt%) Au onto the CeO_2–ZrO_2 support. The appropriate amount of hydrogen tetrachloroauric (III) acid trihydrate ($HAuCl_4{\cdot}3H_2O$; 99.5%, Merck, CAS 16961-25-4) was weighed and dissolved in distilled water (DW) under vigorous stirring at 80 °C. The dried support (CeO_2–ZrO_2) was added to the solution, and the pH was adjusted to pH 8–9 by the addition of 0.1 M Na_2CO_3 solution and then aged at 80 °C for 1 h. The precipitate was washed with an excess amount of warm DW, dried at 110 °C for 12 h, and calcined in air at 400 °C for 4 h.

For comparison, pure CeO_2 and ZrO_2 supports were also prepared by precipitation using $Ce(NO_3)_3{\cdot}6H_2O$ and $ZrOCl_2{\cdot}8H_2O$ as precursors. Then, Au/CeO_2 and Au/

ZrO_2 were prepared by DP as described above, except that the CeO_2 or ZrO_2 support was added to the solution.

Catalyst characterization

X-ray diffraction (XRD) analysis

Powder XRD measurements were performed using a Rigaku X-ray diffractometer system (DMAX 2200 HV, Crest Nanosolution Limited, Thailand) with CuKα radiation ($\lambda = 1.5406$ Å) and operated at 40 kV and 30 mA. The intensity data were collected over a 2θ range of 20–80° with a step size of 0.02°min^{-1}. The crystallite size was calculated based on Scherrer's equation, shown in Eq. (1);

$$B(2\theta) = \frac{K\lambda}{\beta \cos}, \tag{1}$$

where β is the line broadening at half the maximum intensity (FWHM), λ is the wavelength (0.154 nm), θ is the Bragg angle ($2\theta = 39.7°$), and K is Scherrer's constant of 0.9 [15]. Information on the Au species was attained by UV–vis spectroscopy, measuring the absorbance over a wavelength of 200–800 nm in a Shimadzu 2550 UV/vis spectrophotometer (Bara Scientific Co., Ltd., Thailand). The absorption intensity was expressed using the Kubelka–Munk function, $F(R\infty) = (1-R\infty)^2/(2R\infty)$, where $R\infty$ is the diffuse reflectance from a semi-infinite layer [16].

Catalyst surface area measurement

Nitrogen (N_2) physisorption isotherms were determined at −196 °C using an Autosorb-1 Gas Sorption System (Quantachrome Corporation). The specific surface areas of catalyst were calculated from the N_2 adsorption data according to the Brunauer–Emmett–Teller (BET) method. Prior to measurement, all samples were degassed at 250 °C for 12 h under a high vacuum condition to remove any surface adsorbed residues.

Catalyst reducibility by H_2-temperature-programmed reduction (TPR) analysis

The H_2-TPR was performed in a quartz tube reactor using a TPDRO 1100 instrument (Thermo Finnigan) equipped with a thermal conductivity detector (TCD). In each trial, 100 mg of catalyst was preheated from room temperature (RT) to 200 °C under a helium (He) flow of 50 mL min^{-1} for 30 min. After cooling to RT in He, the reduction temperature was raised from RT to 850 °C at a ramp rate of 10 °C min^{-1} under a reducing gas [1:9 (v/v) H_2: argon] at a flow rate of 30 mL min^{-1}.

Fourier transform infrared spectroscopy (FT-IR)

The carbonate species present in the catalysts were identified via FT-IR measurements using a Thermo Nicolet Nexus 670 FTIR spectrometer in absorbance and

transmittance mode at 32 scans with a resolution of 4 cm^{-1}. To determine the formation of oxygen vacancies, Fourier transform Raman spectra (FT-Raman) of the samples were obtained using a Perkin Elmer (Spectrum GX) FT-Raman spectrometer with an Nd-YAG laser (1064 nm) in absorbance mode. In total, 2000 scans with a resolution of 16 cm^{-1} were used to cover a frequency range of 3500–200 cm^{-1}.

Atomic absorption spectroscopy (AAS)

A Varian model SpectrAA 300 atomic absorption spectrometer was used for measuring the Au content in an air-acetylene flame.

Catalytic activity measurements

Catalytic activity measurements in the CO-PROX reaction were performed in a fixed-bed quartz micro-reactor containing 100 mg of the respective sample at a reaction temperature range of 50–190 °C under atmospheric pressure. The reactant consisted of, all (v/v), 1% CO, 1% oxygen (O_2), 40% H_2, and 58% He, and was passed through the catalyst bed at a total flow rate of 50 mL min^{-1} (gas hourly space volume [GHSV] = 30,000 mL g^{-1} h^{-1}). The product gases were analysed by on-line gas chromatography (GC; HP 5890) equipped with a packed carbosphere column, 80/100 mesh, and 10 ft × 1/8 inch and a TCD. The CO conversion level was based on the CO consumption and the selectivity of carbon dioxide (CO_2) was calculated from the carbon and oxygen mass balance.

Results and discussion

Catalyst characterization

Representative XRD patterns of the 1 wt% Au/$Ce_{1-x}Zr_xO_2$ supports are presented in Fig. 1, where the XRD pattern of CeO_2 corresponded to a face-centred cubic, fluorite-type structure and that of ZrO_2 corresponded to both a monoclinic and tetragonal one. For pure CeO_2, eight characteristic diffraction peaks were detected at 28.5°, 32.9°, 47.4°, 56.2°, 58.8°, 69.2°, 76.6°, and 78.8°, which are indexed to (111), (200), (220), (311), (222), (400), (331), and (420) crystal faces, respectively [14]. The diffraction peaks were shifted slightly to higher diffraction angles and the peaks became broader, or of lower intensity, with the incorporation of increasing amounts of ZrO_2 into CeO_2. This reflects that the Zr^{4+} cation (ionic radius 0.84 Å) had a smaller radius than the Ce^{4+} cation (ionic radius 0.97 Å), and indicated the formation of a solid solution. This is in accord with previous studies, where an increased ZrO_2 content in the CeO_2–ZrO_2 supports resulted in the presence of bulk defects or distortions in the oxygen sublattice [17]. However, the Au peaks, such as Au (111) at 38.5°, were not very distinct in all the supported Au catalysts, suggesting that the AuNPs were well dispersed on the support, of a small size, or at a relatively low content [18].

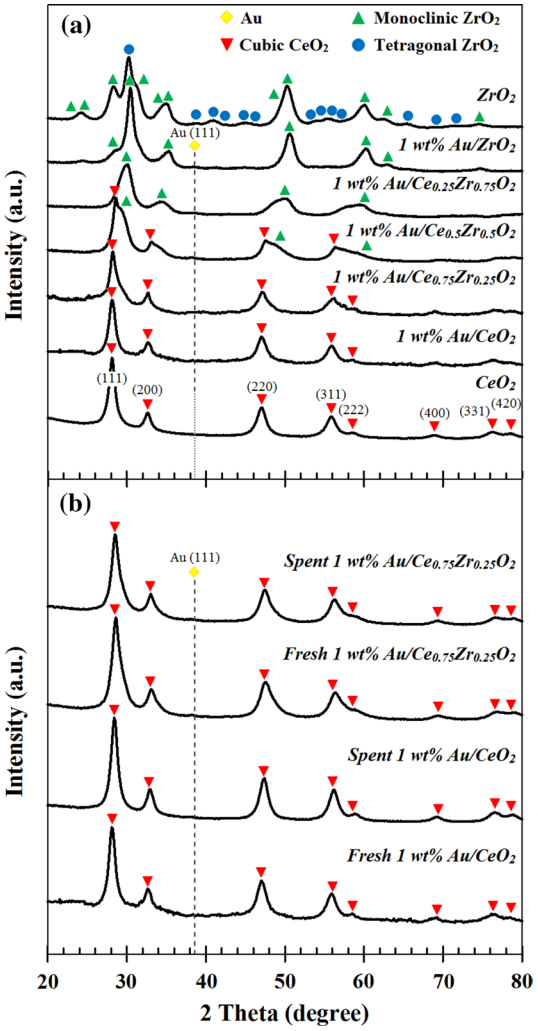

Fig. 1 Representative XRD patterns of the **a** supported Au catalysts and supports and the **b** fresh and spent supported Au catalysts

The actual Au loading level of the 1 wt% Au/CeO_2–ZrO_2 catalysts was measured by AAS, and was found to be lower than the nominal Au loading level (Table 1), presumably due to the non-attachment of the Au complex anions ($[AuCl(OH)_3]^-$ and $[Au(OH)_4]^-$) on the support surface [19]. However, the actual amount of Au deposited on CeO_2 was higher than that on Au/ZrO_2. For the CeO_2–ZrO_2 supports, the actual amount of Au deposited decreased with increasing Zr contents, which might reflect that the Au deposition depended on the point of zero charge (PZC) value and the surface charge of the support. The PZC values for pure CeO_2 and ZrO_2 were 7.72 and 4.87, respectively. If the PZC value of the support is higher than the pH of the solution, the surface will be positively charged (protonation of the surface hydroxyls), resulting in electrostatic adsorption of the Au complex anions. Whereas, if the PZC value of the support is lower than the pH of the solution, the surface

Table 1 Chemical–physical properties of the $Au/CeO_2–ZrO_2$ catalysts

Catalyst	Actual Au loading[a] (%)	Surface area[b] (m^2/g)	Crystallite size[c] (nm)	Lattice constant[d] (nm)		I_{598}/I_{493}^{e}
			CeO_2	CeO_2 (111)	CeO_2 (200)	
Fresh						
CeO_2	n/a	n/a	7.60	0.550	0.550	–
1 wt% Au/CeO_2	0.97	106.6	7.56	0.549	0.550	0.018
1 wt% $Au/Ce_{0.75}Zr_{0.25}O_2$	0.98	121.5	5.59	0.548	0.549	0.039
1 wt% $Au/Ce_{0.5}Zr_{0.5}O_2$	0.96	127.8	4.38	0.543	0.542	–
1 wt% $Au/Ce_{0.25}Zr_{0.75}O_2$	0.87	129.6	2.65	0.518	0.518	–
1 wt% Au/ZrO_2	0.60	169.0	–	–	–	–
Spent						
1 wt% Au/CeO_2	n/a	n/a	7.60	0.544	0.544	0.290
1 wt% $Au/Ce_{0.75}Zr_{0.25}O_2$	n/a	n/a	5.83	0.544	0.547	0.072

All of the samples were calcined at 400 °C. Data are shown as the mean, derived from three different trials

[a]The percentage of each metal was measured quantitatively by AAS

[b]The surface area was measured by BET

[c]The mean crystallite sizes were calculated from the average values of the (111), (200), (220), and (311) CeO_2 planes

[d]The unit cell parameters, as calculated from Bragg's equation

[e]Calculated from the intensity ratio of FT-Raman bands at 463 and 598 cm^{-1}

will be negatively charged (removal of protons from the surface hydroxyls) resulting in the electrostatic repulsion of the Au complex anions [11, 20]. In this study, the solution was adjusted to pH 8 for precipitation, and so the pH was higher than the PZC value of the support. Therefore, in the case of the mixed oxide support, the PZC value of $CeO_2–ZrO_2$ decreased with an increasing Zr content leading to a stronger repulsive force. Thus, the highest Au loading was obtained for the 1 wt% $Au/Ce_{0.75}Zr_{0.25}O_2$ catalyst.

The BET surface areas of the prepared catalysts (Table 1) showed that Au supported on pure CeO_2 and ZrO_2 supports had surface areas of 106.6 and 169.0 m^2/g, respectively, while on the mixed oxide supports they had surface areas in the range of 121.5–129.6 m^2/g, which were between those of the individual CeO_2 and ZrO_2 supports. Among these $Au/CeO_2–ZrO_2$ catalysts, the surface area seemed to increase with an increasing Zr content in the mixed oxides, implying that the surface area of the catalysts was influenced by the substitution of Ce^{4+} with Zr^{4+} ions [21]. It has previously been reported that variation in the Ce/Zr composition led to the formation of a $Ce_{1-x}Zr_xO_2$ solid solution, where the smaller Zr^{4+} ion incorporated and/or substituted inside the larger Ce^{4+} lattice to cause shrinkage in both the ceria lattice and crystallite size [22]. The crystallite size was small when the Zr content was high, which is supported in this study by the fact that the mixed Ce/Zr oxide had a smaller crystallite size (2.65–5.59 nm) than the pure CeO_2 (7.56 nm). The shifting of the CeO_2 diffraction peaks towards

higher angles led to a decreased CeO_2 lattice constant from 0.549 nm for Au/CeO_2 to 0.518 nm for Au/$Ce_{0.25}Zr_{0.75}O_2$. As mentioned previously, the solid solution formation in the mixed Ce/Zr oxide support was considered as one of the main factors to improve the surface area. On the other hand, many studies have reported that the substitution of ZeO_2 into the CeO_2 structure slightly decreased the surface area [23].

To identify the Au species (Au^{3+}, Au cluster, and Au^0) of the catalyst, UV–visible spectroscopy was used and the results are presented in Fig. 2. The pure CeO_2 and ZrO_2 showed a band around 370 nm and 208–210 nm, respectively. For the mixed oxide support, the peak in the range of the CeO_2 and ZrO_2 band was observed at 260–290 nm, according to the full connectivity of Ce–Zr–O linkages via incorporation of Zr into the Ce lattice [24]. Moreover, the peak of CeO_2 shifted to a lower wavelength after adding Zr, which was probably caused by the Zr incorporation. The peak of ZrO_2 became strongly visible at 209–240 nm at higher atom ratios of Zr, implying that it was possible to cause the formation of CeO_2–ZrO_2 solid solution.

The absorption band of Au clusters (Au_n; $1 < n < 10$) and metallic Au (or plasmon, Au^0) can be assigned at 280–300 nm [25] and 500–600 nm [26], respectively, while cationic gold (Au^{3+}) can be observed at a lower wavelength band at around 250 nm [27]. The AuNPs (plasmon) appeared at 353 nm, but the gold clusters and cationic gold species were not clearly observed because the Au species band appeared in the range of the oxide support. Therefore, it was difficult to assign the gold species on the Au/CeO_2–ZrO_2 catalysts using UV–vis spectroscopy. Furthermore, multiple peaks in the UV spectra, which were likely related to the charge transfer transitions, were observed. For example, the band at 275–375 nm can be ascribed to $Ce^{4+} \leftarrow O_2$, while a $Ce^{3+} \leftarrow O_2$ and/or $Zr^{4+} \leftarrow O_2$ charge transfer appeared at 228–275 nm [28]. Nevertheless, this technique can be

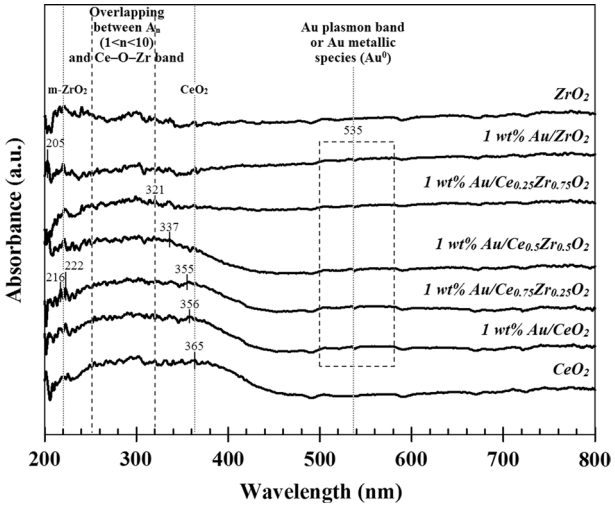

Fig. 2 Representative diffuse reflectance UV–vis spectra of catalysts with various support compositions

used to infer the change in the mixed oxide, which could be attributed to the formation of a solid solution. Moreover, the catalytic activity could relate to the gold species, in which both Au^0 and Au^{3+} species play an important role [29].

The H_2-TPR profile was used to evaluate the reducibility of the catalysts, as shown in Fig. 3. The pure CeO_2 support presented two reduction peaks. The first reduction peak at a low temperature (476 °C) was ascribed to the reduction of oxygen on the ceria surface $Ce^{4+} \rightarrow Ce^{3+}$, while the other one at a higher temperature (836 °C) generally corresponded to the reduction of bulk CeO_2. However, no ZrO_2 reduction peak was observed for the pure ZrO_2 support in the studied temperature range. In the presence of Au, the reduction profiles of the Au catalysts shifted to a lower temperature, and the appearances of the lowest reduction peaks at 77–100 °C corresponded to the reduction of Au_xO_y species (or Au hydroxide) [30]. For Au/CeO_2, it has been suggested that Au modified the properties of CeO_2 by enhancing the reducibility of CeO_2 surface oxygen, which caused a decreased strength of the surface Ce–O bonds adjacent to the gold atoms [31], and so led to an increased surface lattice oxygen mobility and reducibility. Moreover, the reduction peak of the support also shifted to a lower temperature, due to the strong interaction between the metal and support [32]. In the TPR profiles of the Au/CeO_2–ZrO_2 supports, the shift in the reduction of bulk CeO_2 from 836 °C to lower temperatures resulted from the creation of oxygen vacancies due to the solid solution formation [33]. Similar low-temperature shifts in the reduction of supports by the presence of Ni and Au metals have frequently been reported due to the hydrogen spill over effect [34, 35].

The area under the reduction peak can be related to the amount of reducible surface oxygen species. Since Au^0 is normally less reductive than $Au^{\delta+}$, the presence of Au^0 results in less H_2 consumption in the reduction process compared to that with $Au^{\delta+}$. When focusing on the change in the Au reduction area with increasing Zr content, it was found that the H_2 consumption (or area/intensity) decreased significantly

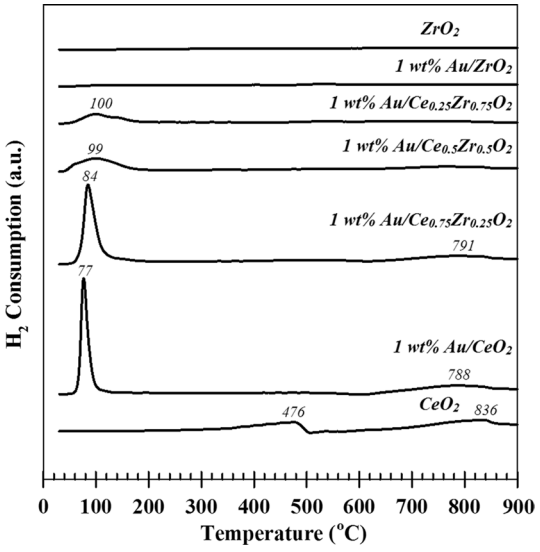

Fig. 3 Representative H_2-TPR profiles of the CeO_2, ZrO_2, Au/CeO_2, Au/ZrO_2, and Au/CeO_2–ZrO_2 catalysts with various support compositions

when increasing the Zr atomic ratio from 25% to 75%. This suggested that the generation of Au^0 species was more favourable in the Zr-rich catalysts. As to the existence of Au^0 species with excess Zr^{4+}, the excess Zr^{4+} possibly dissolved inside the $Au^{\delta+}$ to form an Au_n cluster or Au^0 species [36]. Not only the reduction area but also the position of the Au reduction peak changed, shifting towards a higher temperature (77 to 100 °C), with higher Zr contents. This represented the strengthening of the metal-support (Au-support) interactions, while the existence of two reduction peaks at a temperature range of 50–200 °C might indicate the different gold species. Hence, it was reasonable to speculate that the changes in the amount of Au^0 and Zr content as being due to the Zr^{4+} solubility inside the $Au^{\delta+}$ after forming the strong interaction. However, the exact amounts of Au^0 and $Au^{\delta+}$ were not determined in this study since the gap difference in the Au reduction area was not large enough to measure this species.

When correlating the variety of Au species to the catalytic activity, several previous studies have found that active catalysts always contained metallic Au^0 particles [8], whereas the high activity AuNPs contained the coexistence of $Au^{\delta+}$ and Au^0 species [37]. In this work, both Au^0 and $Au^{\delta+}$ species likely acted as the catalytic active site, with $Au^{\delta+}$ acting as the dominant active species but the combination of Au^0 and $Au^{\delta+}$ being responsible for the active sites in the reaction. The metallic Au^0 activated the O_2 and hydroxyl molecules, while the gold cation (Au^{3+}) linked the metallic Au^0 on the support and provided the pathway for the reaction [38]. This agrees with the UV–vis analysis.

Catalytic activity measurement

The effect of the support composition was varied as 1 wt% Au/$Ce_{1-x}Zr_xO_2$ (x = 0, 0.25, 0.5, 0.75, or 1) and the catalytic activity, in terms of the CO conversion level and selectivity towards CO oxidation, of the 1 wt% Au/$Ce_{1-x}Zr_xO_2$ catalysts was examined. The catalytic activity depended on the Ce/Zr atomic ratio of the oxide support, where the 1 wt% Au/CeO_2 and 1 wt% Au/ $Ce_{0.75}Zr_{0.25}O_2$ catalysts had a similar catalytic performance, in that they had a high activity at a low temperature that then decreased with increasing temperature (Fig. 4). The trend for these two catalysts was quite similar to that reported for a Au/CeZr10 catalyst, which gave a maximum CO conversion level of 65% at 75 °C in a reaction mixture containing, all (v/v), 2% CO, 1% O_2, 50% H_2, and 47% N_2 [39].

In contrast, the catalytic activity of the 1 wt% Au/$Ce_{0.5}Zr_{0.5}O_2$, 1 wt% Au/$Ce_{0.25}Zr_{0.75}O_2$, and 1 wt% Au/ZrO_2 catalysts increased with increasing temperature until they reached a maximum CO conversion level and thereafter began to decrease. That there was a decreased selectivity at higher temperatures reflects the higher activation energy for H_2 oxidation than for CO oxidation [40], and the Ce-rich catalyst gave a stable selectivity with changing operating temperatures.

The maximum CO conversion level for a 1 wt% catalyst was obtained at 50 °C for Au/CeO_2 (92.4% with 48.4% selectivity) and Au/$Ce_{0.75}Zr_{0.25}O_2$ (94.1% with 49.1% selectivity), 70 °C for Au/$Ce_{0.5}Zr_{0.5}O_2$ (85.6% with 42.3% selectivity), and 90 °C for Au/$Ce_{0.25}Zr_{0.75}O_2$ (61.7% with 30.4% selectivity) and Au/ZrO_2 (53.7% with 31.5%

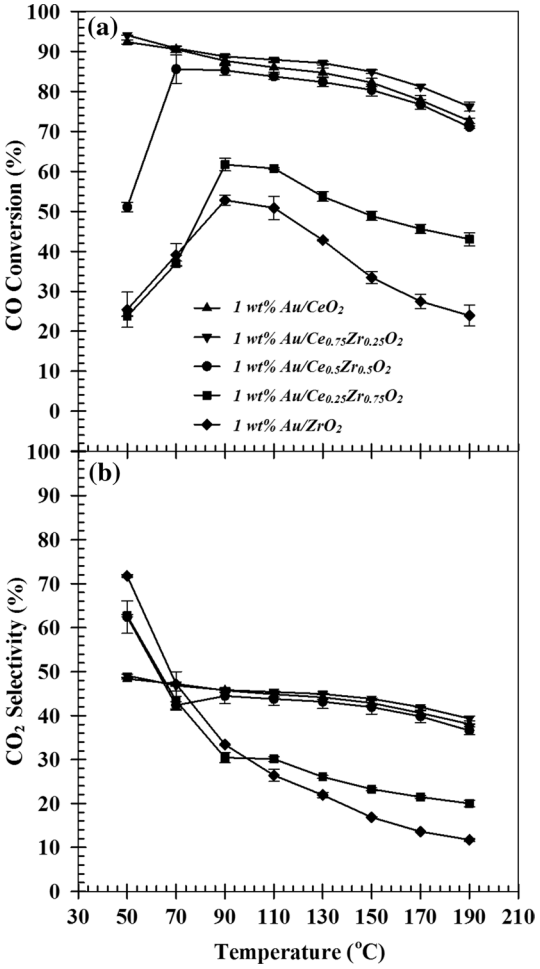

Fig. 4 Catalytic activities of the 1 wt% Au/CeO_2–ZrO_2 catalysts with various Ce/Zr atomic ratios, shown as the **a** CO conversion level and **b** CO_2 selectivity. Data are shown as the mean ± SD, derived from three different trials. Reaction conditions, all (v/v): 1% CO, 1% O_2, 40% H_2, and 58% He; GHSV = 30,000 mL g^{-1} h^{-1}

selectivity). Thus, the support had a significant effect on the catalytic performance, where the catalytic activity (all at 1 wt%) could be ordered as $Au/Ce_{0.75}Zr_{0.25}O_2 \geq Au/CeO_2 > Au/Ce_{0.5}Zr_{0.5}O_2 > Au/Ce_{0.25}Zr_{0.75}O_2 > Au/ZrO_2$. While the incorporation of Zr was beneficial for an enhanced oxygen mobility, the performance of the catalyst depended on an appropriate Zr content. In this work, the 1 wt% $Au/Ce_{0.75}Zr_{0.25}O_2$ catalyst exhibited a slightly higher catalytic activity than the 1 wt% Au/CeO_2 one at a high temperature. It was previously revealed that the $Ce_{1-x}Zr_xO_2$ composite with a low Zr content exhibited a good OSC and high oxygen mobility [41]. The high H_2 consumption peak of the $Au/Ce_{0.75}Zr_{0.25}O_2$ catalyst can be attributed to the better reducibility, suggesting better redox properties as well as a better thermal stability of the prepared catalyst. This can be ascribed to the fact that the AuNPs at the surface might be preferentially in contact with Ce/Zr more than with Ce atoms.

Consequently, the highest catalytic activities for the 1 wt% Au/$Ce_{0.75}Zr_{0.25}O_2$ catalyst could be attributed to the improved catalytic activity and increased oxygen vacancies of the solid solution, as confirmed by the XRD and FT-Raman analyses. The presence of oxygen vacancies allowed a more effective O_2 adsorption and activation for CO oxidation [42]. Therefore, the $Ce_{1-x}Zr_xO_2$ material with a low Zr content exhibited a larger amount of oxygen vacancies than the pure CeO_2, which was found to enhance the oxygen mobility and promoted a high OSC. In addition, the presence of the highest amount of Au deposited on the support may promote the reaction. Furthermore, the catalytic performance could be attributed to the gold species of the catalyst, where both Au^0 and Au^{3+} were responsible for the activity. In this work, the 1 wt% Au/$Ce_{0.75}Zr_{0.25}O_2$ exhibited the highest activity and had the coexistence of $Au^{\delta+}$ and Au^0 species on the support.

It was clearly seen that these catalysts exhibited a high CO conversion level and a high selectivity compared to previous reports for other catalysts with a comparable feed composition and reaction conditions. For example, Au/CeO_2–ZrO_2 catalysts, where the support was synthesized by a pseudo sol–gel method [43], exhibited a 95% CO conversion level at a high temperature (100–150 °C) under reaction conditions that consisted of, all (v/v), 2% CO, 2% O_2, 50% H_2, and 46% He, whereas the temperature for the maximal catalytic activity of Au/CuO–CeO_2 was 50 °C under a feed composition of, all (v/v), 1.33% CO, 1.33% O_2, 65.33% H_2, and 32% He [44]. The catalytic performances of the supported Au catalysts were comparable to or even better than those supported on different materials and other conventional catalysts from previous studies [45–48], with representatives shown in Table 2. Most of the catalysts reached a high catalytic activity with a 90–100% CO conversion level, but the temperature required to attain the maximum CO conversion level of our catalyst can be achieved at a lower temperature of 50 °C.

Effect of water vapour and CO_2

In the present work, the reaction was performed at a constant 50 °C or 110 °C with time-on-stream. The effect of 10% (v/v) CO_2 and 10% (v/v) H_2O on the CO conversion level and selectivity of the 1 wt% Au/$Ce_{0.75}Zr_{0.25}O_2$ catalysts was evaluated at 50 °C and 110 °C (Fig. 5). Although the highest activity was obtained at 50 °C, it has previously been suggested that the presence of water in the feed stream leads to a high CO conversion level at a reaction temperature above 100 °C [49]. The higher activity at 110 °C than at 50 °C was due to the WGS reaction ($H_2O + CO \leftrightarrow H_2 + CO_2$) [50]. In contrast, the best result was obtained at a low temperature for the Au/ZnO and Au/ZnO–Fe_2O_3 catalysts [51].

The temperature was found to have a significant effect on the performance of both the CO conversion level and selectivity. In the presence of H_2O or CO_2 in the feed stream, a lower CO conversion level and higher selectivity were obtained at the low temperature (50 °C) compared to at 110 °C. However, the effect of CO_2 and H_2O is controversial due to the competitive adsorption of both H_2O and CO_2 on the active sites. Generally, CO_2 negatively affects the CO conversion and selectivity, while the addition of H_2O sometimes results in a positive and at other times in a negative effect on the CO conversion. That the CO oxidation activity increased at

Table 2 Comparison of the catalytic performance of different catalysts for PROX

Catalyst	Maximum conversion (%)	Maximum conversion temperature (°C)	Gas composition	References
Au/CeO_2	92	50	1% CO, 1% O_2, 40% H_2, and 58% He	This work
$Au/Ce_{0.75}Zr_{0.25}O_2$	94	50	1% CO, 1% O_2, 40% H_2, and 58% He	This work
Au/CeO_2–ZrO_2 catalysts	95	100–150	2% CO, 2% O_2, 50% H_2, and 46% He	[43]
Au/MnO_x–CeO_2	90	120	1.5% CO, 1.5% O_2, 50% H_2, and balance He	[45]
MnO_2/CO_3O_4 (Mn/Co = 1/8)	100	125	1% CO, 1% O_2, 50% H_2, and 48% He	[46]
$CuO/CeO_2/Al_2O_3$	99	200	0.6% CO, 0.6% O_2, 30% H_2, and balance He	[47]
CuO/CeO_2	97	120	1.25% CO, 1.25% O_2, 50% H_2, and balance He	[48]

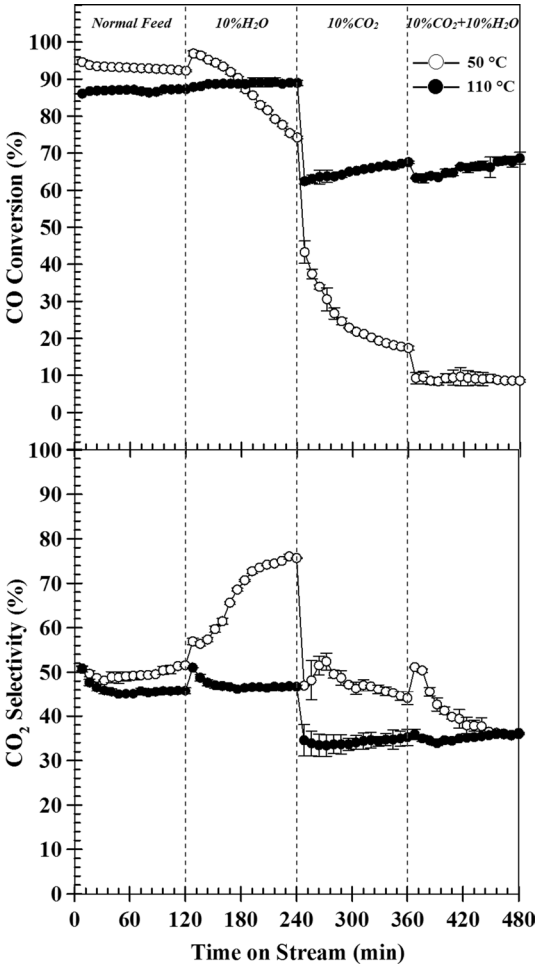

Fig. 5 Effect of temperature in the presence of 10% (v/v) CO_2 and 10% (v/v) H_2O on the catalytic activities of the 1 wt% Au/$Ce_{0.75}Zr_{0.25}O_2$. The reaction was tested at a constant temperature of 50 °C or 110 °C and monitored with time-on-stream

temperatures lower than 120 °C was ascribed to the improved control of the redox reactions, whereas the effect of H_2O is negative at higher temperatures [52].

The addition of H_2O in this work dramatically decreased the CO conversion level at 50 °C, whereas at 110 °C the CO conversion level remained almost the same as in the dry feed stream. The CO conversion level has been reported to strongly depend on the H_2O vapour content, where a negative effect on CO oxidation was noted with a higher H_2O vapour content of up to 6000 ppm [49]. In this study, the CO conversion level was rapidly decreased upon adding CO_2 to the feed stream at both temperatures studied, but with a greater impact at the low temperature (50 °C). The addition of both CO_2 and H_2O had a significant negative impact on the catalytic activity at the low temperature (50 °C), where CO_2 had a more negative effect than H_2O. Although the selectivity was increased at 50 °C, the O_2 conversion level was lower at 50 °C than at 110 °C. So, the O_2 consumption in the conversion of CO to CO_2 was

lower at 50 °C and the selectivity had no significant effect on the activity compared with the CO conversion level. This result agrees well with a previous report that the addition of 2% (v/v) H_2O and 2% (v/v) CO_2 in the feed stream reduced the activity of the $Au/CeO_2–ZrO_2$ catalyst [43].

The water vapour may condense on the catalyst surface and block the active sites. On the other hand, it will dissociate to form OH, and react with CO to produce formate and subsequently decompose to H_2 and CO_2 [53]. The formation of carbonate and formate species was higher at 50 °C than at 110 °C, as evidenced in the FT-IR results. Therefore, the accumulation of these species could block the active sites and so have a significant inhibitory effect on the catalytic performance in the CO-PROX reaction.

Catalysts stability (deactivation test)

The stability of the 1 wt% Au/CeO_2 and 1 wt% $Au/Ce_{0.75}Zr_{0.25}O_2$ catalysts was evaluated in dry and wet conditions at a reaction temperature of 110 °C for 33 h (Fig. 6). Both the 1 wt% Au/CeO_2 and 1 wt% $Au/Ce_{0.75}Zr_{0.25}O_2$ catalysts exhibited a good stability in the simulated dry condition and showed similar results, maintaining their activities without loss for 28 h. However, in the simulated wet condition their stability, as determined by the CO conversion level and CO_2 selectivity relative to the fresh catalyst, was significantly decreased to 70% after 5 h, due to the formation of carbonate and formate species from CO_2 and H_2O. However, they otherwise exhibited the same results as the fresh catalysts and maintained a 70% relative activity during the reaction time. In contrast, Au/Fe_2O_3 and Au/TiO_2 were reported to lose their initial catalytic performance during the first hours of reaction. It is known that a strong metal–support interaction might lead to catalyst deactivation. The support is partially reduced under reaction conditions and has a high affinity for the metal particles to fully cover the active surface of metal particles.

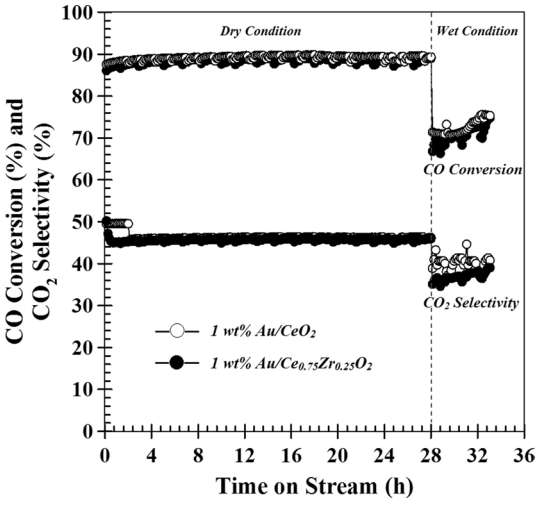

Fig. 6 Deactivation test of the 1 wt% Au/CeO_2 and 1 wt% $Au/Ce_{0.75}Zr_{0.25}O_2$ catalysts. Reaction conditions, all (v/v): 1% CO, 1% O_2, 40% H_2, and 58% He for the dry condition and 1% CO, 1% O_2, 40% H_2, 10% H_2O, 10% CO_2, and 38% He for the wet condition

Figure 1b shows a comparison of the representative XRD patterns between the fresh and spent (33 h reaction time) 1 wt% Au/CeO_2 and 1 wt% Au/$Ce_{0.75}Zr_{0.25}O_2$ catalysts. The spent catalyst had almost the same XRD pattern as that of the fresh catalyst, implying that there was no change in the crystallite structure of both Au and CeO_2 [54]. There was a small increase in the CeO_2 crystallite size for both the 1 wt% Au/CeO_2 (7.56 to 7.60 nm) and 1 wt% Au/$Ce_{0.75}Zr_{0.25}O_2$ (5.59 to 5.83 nm). No Au reflection peak was observed in both the fresh and spent catalysts. Considering the lattice constants of the spent catalysts, both the 1 wt% Au/CeO_2 and 1 wt% Au/$Ce_{0.75}Zr_{0.25}O_2$ showed a decreased lattice constant from 0.550 to 0.544 nm and from 0.548 to 0.545 nm, respectively. It has been suggested that the gas feeding stream possibly affected the ceria lattice, where it varied significantly, being increased after exposure to CO and decreased after exposure to H_2O [55]. Therefore, this could be related to the complex mechanisms during the reaction that changed the CeO_2 lattice and helped restructure the solid solution phase. Regardless, the exact mechanism is still unclear for the solid solution recovery.

Representative FT-Raman spectra of the fresh and spent Au/CeO_2 and Au/$Ce_{0.75}Zr_{0.25}O_2$ catalysts are presented in Fig. 7. The main band at 463 cm^{-1} corresponded to the oxygen vibrations around each Ce^{4+} cation in the metal oxides (F2g mode), and the weak band at around at 598 cm^{-1} was associated with the formation of oxygen vacancies in the ceria lattice [22, 56]. The oxygen vacancies increased after exposure to the CO-PROX reaction, and, as these provide the reaction sites for the reaction, this led to an excellent catalytic stability. The presence of oxygen vacancy sites was also previously confirmed by FT-Raman studies of (Ce–La–xCu)O_2 catalysts with well-dispersed Cu–O species [57]. The ZrO_2 bands typically appeared at 176, 380, 475, and 640 cm^{-1} for the monoclinic phase and at 266, 313, 470, and 640 cm^{-1} for the tetragonal phase [58].

In the case of Zr incorporation, the weak bands of zirconia appeared at around 380 and 313 cm^{-1} and no strong FT-Raman peaks of zirconia were observed, which

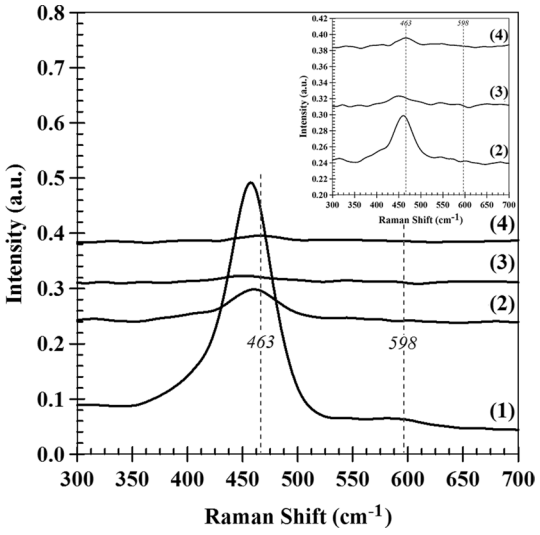

Fig. 7 Representative FT-Raman spectra of the (1, 2) fresh and (3, 4) spent (1, 3) 1 wt% Au/CeO_2 and (2, 4) Au/$Ce_{0.75}Zr_{0.25}O_2$ catalysts

is in accord with the XRD measurements of $Au/Ce_{0.75}Zr_{0.25}O_2$. The incorporation of the Zr^{4+} cation into the lattice of CeO_2 resulted in a broadening of the F2g band (Fig. 7, lines 1 and 2), which is related to the decreased crystallite size or lattice constant [59], and shifted to higher wave numbers, where the intense bands were attributed to the overlapping of the CeO_2 and ZrO_2 phases. A marked decrease in intensity of the FT-Raman band at 463 cm^{-1} was observed, which likely depended on several factors, including the grain size and morphology. The band at 598 cm^{-1} disappeared for the doped catalyst due to the interaction of Zr^{4+} ions placed at interstitial positions of the fluorite structure with the oxygen vacancies [60].

In addition, the intensity ratio of the band of oxygen vacancies and the F2g mode of the fluorite-type structure (I_{598}/I_{463}) were also calculated to evaluate the amount of oxygen vacancies in the sample, with the results shown in Table 1. The intensity ratio increased with increasing incorporation levels of Zr, implying that doping of Zr in CeO_2 increased the concentration of oxygen vacancies due to the change in the lattice structure of CeO_2 by substitution of Ce^{4+} with Zr^{4+}. This change can promote lattice deformation and the formation of oxygen vacancies. In general, an oxygen vacancy is produced by the reduction of the cationic Ce^{4+} to Ce^{3+}. The addition of the smaller Zr^{4+} atoms could provide some spare space for accommodating the bigger Ce^{3+} cations and increasing the formation of an oxygen vacancy [12].

Moreover, the intensity ratio of the fresh catalysts was lower than that for the spent catalysts, indicating that it may have acquired some defect structure or restructure during the reaction. This defect could have resulted from lattice parameter changes and increased oxygen vacancies. These results are not in accord with previous work on supported Au catalysts in the OSRM [13] and for a $CeZrO_{4-\delta}$ oxide catalyst in the oxidative dehydrogenation of ethylbenzene to styrene [61]. The intensity ratio of both fresh catalysts increased markedly after exposure to the CO-PROX reaction, implying that the concentration of the oxygen vacancies in the CeO_2–ZrO_2 support was dramatically increased. The disappearance of the weak peak at 313 cm^{-1} (Fig. 7, lines 2 and 4) of the spent $Au/Ce_{0.75}Zr_{0.25}O_2$ suggested the displacement of oxygen atoms from fluorite lattice positions.

Thus, the FT-Raman and XRD analyses revealed a change in the CeO_2 lattice in the presence of Zr in accord with the formation of solid solutions and an increased number of oxygen vacancies [62]. On the other hand, the reduction of the oxide caused the formation of surface vacancies, which then migrated into the bulk. The reduction progressively emptied the surface of active Ce^{4+} sites, which then limited the amount of oxygen reduction. Although the catalyst surface created more oxygen vacancies, they cannot diffuse O^{2-} in the lattice, which is the rate-determining step [63]. Accordingly, high oxygen vacancies do not per se mean a high catalytic activity due to the limitation of the OSC.

Nevertheless, the FT-IR spectra in Fig. 8 were assigned to species that could block the active sites after the reaction. The FT-IR spectra were observed in two regions, which were a broad band region ascribed to the O–H stretching mode at 2500–3700 cm^{-1} [64] and the second region at 1200–1800 cm^{-1} that was ascribed to the chemisorption of carbonate species [65]. After the catalyst was tested in a simulated wet condition (with $H_2O + CO_2$), the intensity of the O–H peak at 3400 cm^{-1} was higher and broader than that for the fresh catalyst. This may have been caused

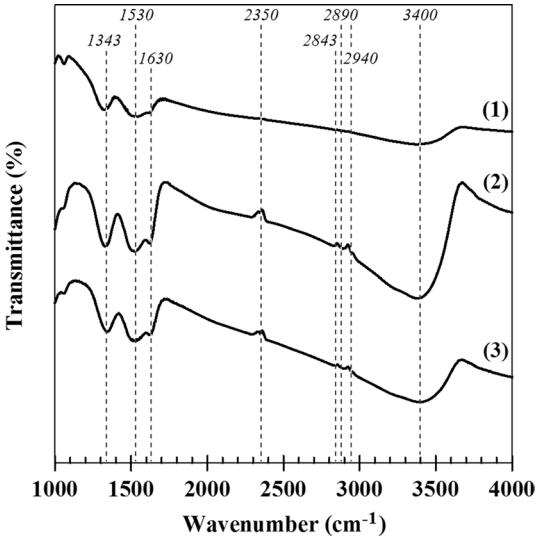

Fig. 8 Representative FT-IR spectra of the (1) fresh and (2, 3) spent 1 wt% Au/$Ce_{0.75}Zr_{0.25}O_2$ catalysts after exposure at (2) 50 °C or (3) 110 °C with a gas composition of, all (v/v): 40% H_2, 1% O_2, 1% CO, 10% CO_2, 10% H_2O, and 38% He

by the presence of undissociated water molecules or the water produced from the oxidation of H_2 on the catalyst surface.

The spent catalysts also showed a strong peak at 1343 cm^{-1}, ascribed to CO molecules adsorbed on the surface by chemisorption. The formation of carbonates is an indication of CO oxidation by surface oxygen species and was presented by bands at 1582, 1413, and 1220 cm^{-1}, assigned to bicarbonate species (HCO_3^-) [53]. Bands were also observed at 1640 cm^{-1}, corresponding to the O–H bending mode of molecular water, and at 2351 cm^{-1}, implying that gaseous CO_2 molecules were linearly adsorbed on the surface cations of the support [53]. Bands at 2840 and 2940 cm^{-1}, which corresponded to the formation of the formate species on the catalyst surface [64], also appeared. In addition, the spent catalysts from different operating temperatures were compared, where at a low temperature (50 °C) there was a stronger accumulation of both carbonate and formate species than at the high temperature (110 °C). This suggested that these species decreased at temperatures above 100 °C and so the temperature had a significant effect on the catalytic activity [64].

Conclusions

A series of Au-based catalysts supported on mixed-metal oxides ($Au/CeO_2–ZrO_2$) were investigated in the PROX reaction in comparison with Au/CeO_2 and Au/ZrO_2. The 1 wt% $Au/Ce_{0.75}Zr_{0.25}O_2$ catalyst, with the coexistence of $Au^{\delta+}$ and Au^0 species on the support, exhibited the highest catalytic activity with a 94.1% CO conversion level and 49.1% PROX selectivity at 50 °C, even in the presence of H_2O and CO_2 in the feed stream. It was found that the incorporation of Zr enhanced the catalytic activity, due to a solid solution formation, and this increased the amount of oxygen vacancies and active oxygen species. The catalytic activity of both the 1 wt% Au/

CeO_2 and 1 wt% $Au/Ce_{0.75}Zr_{0.25}O_2$ catalysts was maintained in a dry condition at 110 °C for 28 h.

Acknowledgements The authors acknowledge the contributions and financial support from the Ratchadaphiseksomphot Endowment Fund, Chulalongkorn University.

References

1. M. Haruta, N. Yamada, T. Kobayashi, S. Iijima, J. Catal. **115**, 301 (1989)
2. Q. Zhang, Y. Zhan, X. Lin, Q. Zheng, Catal. Lett. **115**(3–4), 143 (2007)
3. M. Carltonbird, S. Eaimsumang, S. Pongstabodee, S. Boonyuen, S.M. Smith, A. Luengnaruemitchai, Chem. Eng. J. **344**, 545 (2018)
4. C. Pojanavaraphan, W. Nakaranuwattana, A. Luengnaruemitchai, E. Gulari, Chem. Eng. J. **240**, 99 (2014)
5. A. Luengnaruemitchai, K. Srihamat, C. Pojanavaraphan, R. Wanchanthuek, Int. J. Hydrog. Energy **40**(39), 13443 (2015)
6. M. Susana Moreno, E. López, M. Esperanza Adrover, N.J. Divins, J. Llorca, Int. J. Hydrog. Energy **41**(47), 22043 (2016)
7. S. Carrettin, P. Concepcion, A. Corma, J.M.L. Nieto, V.F. Puntes, Angew. Chem. Int. Ed. **43**, 2538 (2004)
8. L.-H. Chang, N. Sasirekha, Y.-W. Chen, W.-J. Wang, Ind. Eng. Chem. Res. **45**, 4927 (2006)
9. M. Lomello-Tafin, A.A. Chaou, F. Morfin, V. Caps, J.-L. Rousset, Chem. Commun. **3**, 388 (2005)
10. S. Letichevsky, C.A. Tellez, R.R. de Avillez, M.I.P. da Silva, M.A. Fraga, L.G. Appel, Appl. Catal. B Environ. **58**(3–4), 203 (2005)
11. C. Pojanavaraphan, A. Luengnaruemitchai, E. Gulari, Int. J. Hydrog. Energy **38**(3), 1348 (2013)
12. N. Hickey, P. Fornasiero, J. Kašpar, J.M. Gatica, S. Bernal, J. Catal. **200**(1), 181 (2001)
13. A. Luengnaruemitchai, C. Pojanavaraphan, A. Kumyam, C. Thunyaratchatanon, E. Gulari, Int. J. Hydrog. Energy **44**(3), 1686 (2019)
14. C. Pojanavaraphan, A. Luengnaruemitchai, E. Gulari, Appl. Catal. A Gen. **456**, 135 (2013)
15. A. Patterson, Phys. Rev. **56**(10), 978 (1939)
16. G. Kortüm, *Reflectance Spectroscopy* (Springer, Berlin, 1969)
17. J.A. Rodriguez, X. Wang, J.C. Hanson, G. Liu, A. Iglesias-Juez, M. Fernández-García, J. Chem. Phys. **119**(11), 5659 (2003)
18. A. Luengnaruemichai, D.T.K. Thoa, S. Osuwan, E. Gulari, Int. J. Hydrog. Energy **30**(9), 981 (2005)
19. C.K. Costello, J.H. Yang, H.Y. Law, Y. Wang, J.-N. Lin, L.D. Marks, M.C. Kung, H.H. Kung, Appl. Catal. A Gen. **243**(1), 15 (2003)
20. F.-W. Chang, T.-C. Ou, L.S. Roselin, W.-S. Chen, S.-C. Lai, H.-M. Wu, J. Mol. Catal. A: Chem. **313**(1–2), 55 (2009)
21. H. Zhang, H. Liu, J. Energy Chem. **22**(1), 98 (2013)
22. B.M. Reddy, A. Khan, Catal. Surv. Asia **9**(3), 155 (2005)
23. I. Dobrosz-Gómez, I. Kocemba, J.M. Rynkowski, Appl. Catal. B Environ. **83**(3–4), 240 (2008)
24. H.-R. Chen, J.-L. Shi, T.-D. Chen, J.-N. Yan, D.-S. Yan, Mater. Lett. **54**(2–3), 200 (2002)
25. K.R. Souza, A.F. de Lima, F.F. de Sousa, L.G. Appel, Appl. Catal. A Gen. **340**(1), 133 (2008)
26. S. Park, K. Yoo, H.-J. Park, J.-C. Lee, J.-H. Lee, J. Electroceram. **17**(2–4), 831 (2006)
27. A.K. Gangopadhayay, A. Chakravorty, J. Chem. Phys. **35**(6), 2206 (2004)
28. A. Kambolis, H. Matralis, A. Trovarelli, C. Papadopoulou, Appl. Catal. A Gen. **377**(1–2), 16 (2010)
29. S.-P. Wang, T.-Y. Zhang, X.-Y. Wang, S.-M. Zhang, S.-R. Wang, W.-P. Huang, S.-H. Wu, J. Mol. Catal. A: Chem. **272**(1–2), 45 (2007)
30. I. Dobrosz-Gómez, M.Á. Gómez-García, J. Rynkowski, Kinet. Catal. **51**(6), 823 (2010)
31. S. Scirè, S. Minicò, C. Crisafulli, C. Satriano, A. Pistone, Appl. Catal. B Environ. **40**(1), 43 (2003)
32. F.-W. Chang, L.S. Roselin, T.-C. Ou, Appl. Catal. A Gen. **334**(1–2), 147 (2008)
33. M.H. Youn, J.G. Seo, K.M. Cho, S. Park, D.R. Park, J.C. Jung, I.K. Song, Int. J. Hydrog. Energy **33**, 5052 (2008)
34. Y. Liu, A.J. McCue, P. Yang, Y. He, L. Zheng, X. Cao, Y. Man, J. Feng, J.A. Anderson, D. Li, Chem. Sci. **10**, 3556 (2019)

35. G. Rochard, J.-M. Giraudon, L.F. Liotta, V.L. Parola, J.-F. Lamonier, Catal. Sci. Technol. **9**, 3203 (2019)
36. C. Pojanavaraphan, A. Luengnaruemitchai, E. Gulari, Int. J. Hydrog. Energy **37**(19), 14072 (2012)
37. M. Han, X. Wang, Y. Shen, C. Tang, G. Li, R.L. Smith Jr., J. Phys. Chem. C **114**(2), 793 (2009)
38. T. Sakwarathorn, A. Luengnaruemitchai, S. Pongstabodee, J. Ind. Eng. Chem. **17**(4), 747 (2011)
39. O.H. Laguna, F. Romero Sarria, M.A. Centeno, J.A. Odriozola, J. Catal. **276**(2), 360 (2010)
40. A. Luengnaruemitchai, S. Osuwan, E. Gulari, Int. J. Hydrog. Energy **29**(4), 429 (2004)
41. Z. Zhao, R. Jin, T. Bao, X. Lin, G. Wang, Appl. Catal. B Environ. **110**(2), 154 (2011)
42. A. Longo, L.F. Liotta, G. Pantaleo, F. Giannici, A.M. Venezia, A. Martorana, J. Phys. Chem. C **116**(4), 2960 (2012)
43. L.F. Córdoba, A. Martínez-Hernández, Int. J. Hydrog. Energy **40**(46), 16192 (2015)
44. D.-S. Lee, Y.-W. Chen, Int. J. Hydrog. Energy **41**, 3605 (2016)
45. Y.B. Tu, M. Meng, Z. Sun, L. Zhang, T. Ding, T. Zhang, Fuel Process. Technol. **93**, 78 (2012)
46. Q. Zhang, X. Liu, W. Fan, Y. Wang, Appl. Catal. B Environ. **102**, 207 (2011)
47. E. Moretti, M. Lenarda, L. Storaro, A. Talon, R. Frattini, S. Polizzi, E. Rodriguez-Castellon, A. Jimenez-Lopez, Appl. Catal. B Environ. **72**, 149 (2007)
48. J.A. Cecilia, A. Arango-Diaz, J. Marrero-Jerez, P. Nunez, E. Moretti, L. Storaro, E. Rodiguez-Castellon, Catalysts **7**, 160 (2017)
49. M. Daté, Y. Ichihashi, T. Yamashita, A. Chiorino, F. Boccuzzi, M. Haruta, Catal. Today **72**(1–2), 89 (2002)
50. M.M. Schubert, A. Venugopal, M.J. Kahlich, V. Plzak, R.J. Behm, J. Catal. **222**(1), 32 (2004)
51. P. Naknam, A. Luengnaruemitchai, S. Wongkasemjit, Int. J. Hydrog. Energy **34**(24), 9838 (2009)
52. M.A. Centeno, C. Portales, I. Carrizosa, J.A. Odriozola, Catal. Lett. **102**(3–4), 289 (2005)
53. F. Boccuzzi, A. Chiorino, M. Manzoli, D. Andreeva, T. Tabakova, J. Catal. **188**(1), 176 (1999)
54. A.C. Gluhoi, H.S. Vreeburg, J.W. Bakker, B.E. Nieuwenhuys, Appl. Catal. A Gen. **291**(1–2), 145 (2005)
55. X. Wang, J.A. Rodriguez, J.C. Hanson, D. Gamarra, A. Martínez-Arias, M. Fernández-García, J. Phys. Chem. B **110**(1), 428 (2006)
56. W.Y. Hernández, F. Romero-Sarria, M.A. Centeno, J.A. Odriozola, J. Phys. Chem. C **114**(24), 10857 (2010)
57. M. AlKetbi, K. Polychronopoulou, A.F. Zedan, V. Sebastián, M.A. Baker, A. AlKhoori, M.A. Jaoude, O. Alnuaimi, S.S. Hinder, A. Tharalekshmy, A.S. AlJaber, Mater. Res. Bull. **108**, 142 (2018)
58. T.A. Maia, J.M. Assaf, E.M. Assaf, Mater. Chem. Phys. **132**(2–3), 1029 (2012)
59. R.C.R. Neto, M. Schmal, Appl. Catal. A Gen. **450**, 131 (2013)
60. F.J. Pérez-Alonso, M. Ojeda, T. Herranz, S. Rojas, J.M. González-Carballo, P. Terreros, J.L.G. Fierro, Catal. Commun. **9**, 1945 (2008)
61. K. Periyasamy, V.T. Aswathy, V.A. Kumar, M. Manikandan, R. Shukla, A.K. Tyagi, T. Raja, RSC Adv. **5**, 3619 (2015)
62. M. AlKetbi, K. Polychronopoulou, M.A. Jaoude, M.A. Vasiliades, V. Sebastian, S.J. Hinder, M.A. Baker, A.F. Zedan, A.M. Efstathiou, Appl. Surf. Sci. **505**, 144474 (2020)
63. M. Boaro, C. De Leitenburg, G. Dolcetti, A. Trovarelli, J. Catal. **193**(2), 338 (2000)
64. D. Gamarra, A. Martínez-Arias, J. Catal. **263**(1), 189 (2009)
65. J. Fan, D. Weng, X. Wu, X. Wu, R. Ran, J. Catal. **258**(1), 177 (2008)